

# Navigating in the Dark: A Multimodal Framework and Dataset for Nighttime Traffic Sign Recognition

Aditya Mishra  
EECS Department  
IISER Bhopal  
aditya21@iiserb.ac.in

Akshay Agarwal  
DSE Department  
IISER Bhopal  
akagarwal@iiserb.ac.in

Haroon Lone  
EECS Department  
IISER Bhopal  
haroon@iiserb.ac.in

## Abstract

*Traffic signboards are vital for road safety and intelligent transportation systems, enabling navigation and autonomous driving. Yet, recognizing traffic signs at night remains challenging due to visual noise and scarcity of public nighttime datasets. Despite advances in vision architectures, existing methods struggle with robustness under low illumination and fail to leverage complementary multimodal cues effectively. To overcome these limitations, firstly, we introduce INTSD, a large-scale dataset comprising street-level night-time images of traffic signboards collected across diverse regions of India. The dataset spans 41 traffic signboard classes captured under varying lighting and weather conditions, providing a comprehensive benchmark for both detection and classification tasks. To benchmark INTSD for night-time sign recognition, we conduct extensive evaluations using state-of-the-art detection and classification models. Secondly, we propose LENS-Net, which integrates an adaptive image enhancement detector for joint illumination correction and sign localization, followed by a structured multimodal CLIP-GCNN classifier that leverages cross-modal attention and graph-based reasoning for robust and semantically consistent recognition. Our method surpasses existing frameworks, with ablation studies confirming the effectiveness of its key components. The dataset and code for LENS-Net is publicly available for research<sup>1</sup>.*

## 1. Introduction

Robust object detection and fine-grained classification remain core challenges in computer vision. Advances in deep learning and visual architectures have achieved remarkable progress across diverse domains [19, 28, 38, 39], supported by large-scale scene understanding datasets [10, 20, 24]. In this work, we focus on Traffic Sign Recognition (TSR),

introducing a new benchmark dataset and a multimodal framework designed for robust detection and classification under challenging nighttime conditions.

Traffic signboards play a critical role in Advanced Driver Assistance Systems (ADAS), autonomous driving, navigation, and smart city systems. However, most existing traffic sign datasets [9, 42, 54] predominantly feature daytime imagery, leaving night-time recognition underexplored. To mitigate this gap, prior studies have employed generative translation or domain adaptation techniques such as CycleGAN [53] and CyCADA [18] to synthesize night-time scenes from daytime data. Yet, these approaches often introduce unrealistic artifacts and fail to capture complex photometric effects (such as glare, reflections, and sensor noise), resulting in a persistent domain gap that hinders robustness in real-world deployment [2, 35, 41]

To address this limitation, we present INTSD, a real-world Indian Nighttime Traffic Sign Dataset. The INTSD covers a wide range of geographical area across India and features 14k+ fully annotated instances, in diverse lighting and weather conditions. It also introduces four additional classes that are frequently misclassified by detection models but are absent in existing benchmarks. The inclusion of natural noise factors such as glare and motion blur, makes it a new standard for traffic sign detection and classification tasks.

TSR has been widely studied in computer vision research [11, 22, 27, 45]. However, these studies have largely been validated on datasets with significant limitations. These benchmarks typically lack nighttime imagery, data from diverse camera sensors, and varied weather conditions. Moreover, the traffic sign classes represented often exclude real-world adversarial examples, such as damaged or partially occluded signs. This presents a gap, underscoring the need for extensive research under more challenging and realistic operational scenarios, particularly in nighttime settings.

Recent advances in Graph Convolutional Neural Networks (GCNNs) have shown significant success in im-

<sup>1</sup><https://adityamishra-ml.github.io/INTSD/>

Table 1. Overview of traffic sign datasets. <sup>‡</sup> TT100K has only 10000 images with signboard in it. <sup>§</sup>video-frames covering only 15,630 unique signs. <sup>¶</sup>45 classes have more than 100 examples. <sup>†</sup> The MVD data set only contains front and back signboard classes. <sup>†</sup> signifies if the dataset contains more than 50% night-time images.

Dataset	Images	Classes	Signs	Attributes	Region	Boxes	Unique	Heavily Nighttime <sup>†</sup>
INTSD	6004	41	14,044	tampered, blur, glare, advertisements, MTSD’s attributes	India	✓	×	✓
MTSD [9]	105,830	400	354,154	occluded, exterior, dummy, out-of-frame, included, ambiguous	Global	✓	✓	×
TT100K [54]	<sup>‡</sup> 100,000	<sup>¶</sup> 221	26,349	×	China	✓	✓	×
MVD [34]	20,000	<sup>†</sup> 2	174,541	×	global	✓	✓	×
BDD100K [52]	100,000	1	343,777	×	USA	✓	×	×
GTSDb [43]	900	43	852	×	Germany	✓	×	×
RTSD [42]	<sup>§</sup> 179,138	156	<sup>§</sup> 104,358	×	Russia	✓	×	×
STS [21]	3777	20	5582	×	Sweden	✓	×	×
LISA [33]	6610	47	7855	×	USA	✓	×	×
GTSRB [44]	×	43	39,210	×	Germany	×	✓	×
BelgiumTS [31]	×	108	8851	×	Belgium	×	×	×

age classification [40, 49] and other domain classification tasks [5, 30, 32], largely due to their inherent ability to model spatial representations. Building on this, along with the proven ability of multimodal learning to fuse complementary data sources for more robust classification [36], we propose LENS-Net, **L**earned **E**nhancement & **N**odal-**S**emantic **N**etwork for TSR. It is based on first detect and then classify principle and features: (i) an adaptive image enhancement based detector and (ii) a structured multimodal CLIP-GCNN based classifier. On INTSD, LENS-Net achieves 92.56% mAP@50 for signboard detection and macro-averaged precision of 78.89% for classification.

In summary, we make the following contributions through this research:

1. We present the first nighttime diverse traffic sign dataset with 6004 images across India. The dataset spans over 14K fully annotated images, covering 41 traffic signboard classes.
2. To our knowledge, we are first<sup>2</sup> to present a structured multimodal model, LENS-Net, that integrates vision-language representations with graph convolutional backbone for traffic signboard classification.

## 2. Literature Review

A wide range of traffic sign datasets support detection and recognition research (see Table 1). Early benchmarks such as GTSRB [44] and GTSDb [43] focused on well-lit, structured settings, while later datasets like SwedishTS [21], BelgiumTS [31], RTSD [42], and TT100K [54] expanded geographic and environmental diversity. Large-scale datasets including MVD [34], BDD100K [52], and

<sup>2</sup>Prior works have explored graph-based reasoning for traffic signs, but none have leveraged multimodal vision-language fusion or prompt-guided graph reasoning.

MTSD [9] introduced complex contextual challenges. Yet, night-time datasets remain scarce, motivating INTSD, a dedicated benchmark for low-light traffic sign detection and recognition.

**Image Enhancement:** The night-time conditions adds noise and taint the computer vision tasks. Prior studies [48] have addressed this through image enhancement techniques aimed at improving visibility before detection. Recent works [4, 29] proposed adaptive and restoration-based frameworks that jointly optimize enhancement and detection., while zero-reference mapping [14] and illumination-aware methods [45] also show notable gains in nighttime perception. Motivated by these advances, our LENS-Net detector integrates adaptive image enhancement, enabling end-to-end illumination correction tuned for sign localization.

**Detection:** Detection has evolved from heuristic color-shape approaches [16, 46] to deep CNN-based architectures. One-stage detectors [26, 28, 37] overcome the slowness of two-stage detectors [6, 13, 25, 39], however, cluttered nighttime signboards still challenge these models, motivating adaptive and illumination-aware detection mechanisms.

**Classification:** Following detection, classification remains a fine-grained visual challenge, as many signs differ only in subtle symbols or numerals (e.g., speed limit 30 vs. 80). CNN-based classifiers have long dominated this space, outperforming earlier hand-crafted pipelines [15, 54], while recent approaches use attention [1, 51] and transformer-based [12] architectures to focus on discriminative regions. Such mechanisms are critical for distinguishing visually similar signs, especially under low-light or degraded conditions. In this work, our CLIP-GCNN based classifier builds upon this insight, combining cross-modal attention with graph-based reasoning for semantically coherent classification.

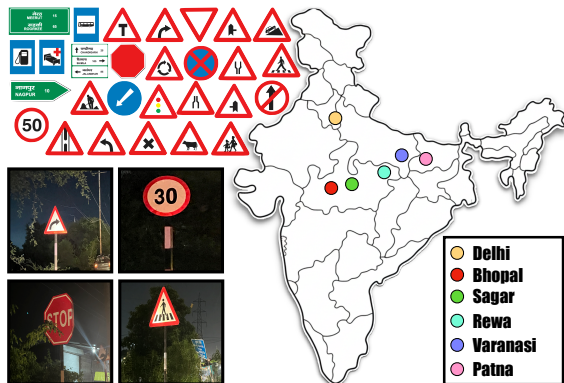


Figure 1. Geographical coverage and representative nighttime traffic sign examples from the INTSD.

### 3. Dataset

The INTSD spans six districts across India, encompassing urban and rural settings and varying environmental conditions such as weather, illumination, motion blur, and glare. Each image contains multiple sign instances, ensuring dense spatial coverage. Figure 1 illustrates representative examples and their geographic distribution. The INTSD also includes challenging scenarios in which signboards are partially occluded by foliage, obscured by other signs, partially out-of-frame, or form part of larger signboards (examples in Appendix 7).

#### 3.1. Data Collection and Curation

The images are primarily extracted from videos recorded at 30fps using a low-budget ( $\approx 60$  USD) action camera (AKASO Ek7000), supplemented with images from various smartphones (Samsung and iPhone), comprising a total of 6004 nighttime images. This mix results in images of varying quality, which we organize into high-quality (smartphone) and low-quality (action camera) subsets. We employed a semi-automated pipeline, iteratively training a YOLOv8 model, to efficiently segregate frames (sampling one frame per second) containing signs from those without signs.

Additionally, INTSD also includes 1,012 day images captured from the same routes. We limit the number of daytime images as they are well-represented in prior Indian datasets [50]. The structured organization (day/night and low/high-quality) makes INTSD useful for image enhancement and for day-to-night image translation tasks for traffic scenes.

#### 3.2. Annotation Process

Annotating traffic signboards is a time-consuming process as it involves selecting and approving images, marking traffic signs with bounding boxes, and assigning appropriate

class label from the predefined Indian MoRTH taxonomy<sup>3</sup>. To increase efficiency, we divide this process into two sequential stages: (i) **Manual annotation**: We manually annotate images using the VGG Image Annotator (VIA) [8]. Following the protocol of MTSD [9], INTSD includes bounding boxes for all traffic-related sign types (e.g., directional, mandatory, informative) and assigns a corresponding class label to each. (ii) **Quality checks**: All annotations in INTSD underwent a strict, triple-verification protocol. Detection errors were minimal: 3.12% false negatives were identified and manually added. A 0.47% labeling error rate observed during the second verification was completely eliminated after the final review.

**Additional Attributes.** In addition to the standard traffic sign classes, we introduce four supplementary classes to address cases that are commonly confused by the TSR models and are not represented in existing datasets: (i) the *tampered* class includes signboards that are broken, rusted, vandalized, or covered with pamphlets; (ii) the *unknown* class comprises of signboards that cannot be mapped to any existing class due to occlusion, motion blur, glare, small size, or partial visibility within the frame; (iii) the *advertisement* class encompasses billboards and other large advertisement boards absent from current datasets; and (iv) the *warning* class contains signboards indicating diversions or other road warnings. INTSD also includes images affected by moderate motion blur and light glare, reflecting real-world conditions (visuals in Appendix 7).

#### 3.3. Statistics

**Class Distribution:** The treemap in Figure 2 (left) illustrates the long-tail class distribution in INTSD. The top five classes: *advertisement* (4,204), *direction* (2,911), *unknown* (1,773), *left\_curve* (855), and *speed* (851), cover most samples. While over half the classes have fewer than 100 instances. Rare but crucial signs such as *airport*, *blow\_horn*, and *cross\_road* are severely underrepresented. This imbalance challenges standard training and motivates the need for methods that learn robust representations across all classes.

**Dataset Distributions:** As illustrated in Figure 2 (right), the dataset statistics present several key challenges. Image sizes follow a bimodal distribution (golden), with distinct clusters around  $\sqrt{area} \approx 1100$  and  $\sqrt{area} \approx 3700$ . Both the signboard sizes (red) and the number of signboards per image (green) exhibit a characteristic long-tail distribution. The majority of signboards are small, and most images contain only 1-4 signs, with an average of 2.32 instances per image. Geographical distribution of INTSD is provided earlier. We defer a detailed analysis of the modeling challenges posed by these distributions to Appendix 7.

<sup>3</sup>[https://morth.nic.in/sites/default/files/road\\_safety\\_books.pdf](https://morth.nic.in/sites/default/files/road_safety_books.pdf)

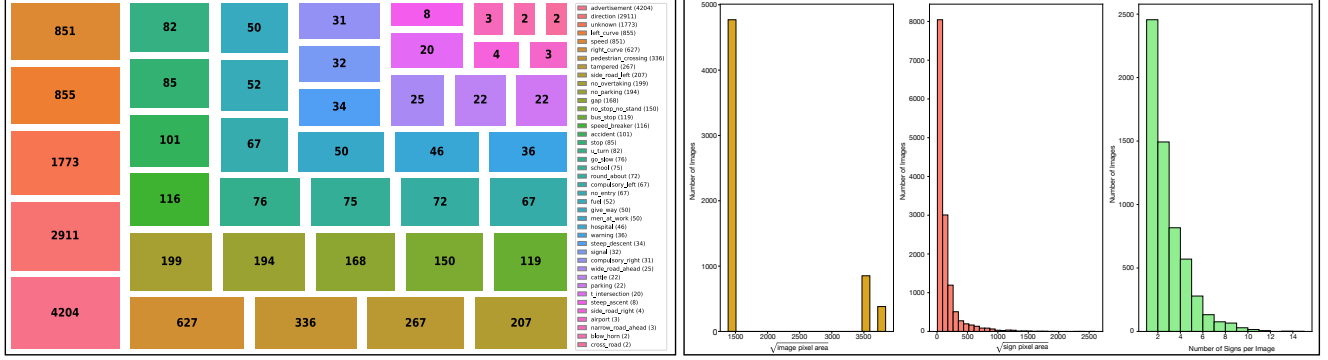


Figure 2. The treemap (on left) illustrates the class distribution. The bar graphs (on right) gives distribution of image size (golden) and signboard size (red) over  $\sqrt{\text{pixel area}}$ , and number of signboards per image (green).

## 4. Method

The proposed method, LENS-Net, comprises of a two-stage architecture designed for robust signboard detection and subsequent fine-grained classification:

- An adaptive pre-processing LENS-Net detector ( $\mathcal{D}$ ) identifies object bounding boxes from a raw image.
- A multimodal graph LENS-Net classifier ( $\mathcal{C}$ ), classifies the content of each cropped bounding box.

This decoupled design allows each stage to be optimized for its specific task:  $\mathcal{D}$  for robust localization under varying imaging conditions, and  $\mathcal{C}$  for high-accuracy classification using deep semantic and attribute-based features. Figure 3 provides an overview of the proposed architecture.

### 4.1. LENS-Net Detector

YOLO models demonstrate strong capability in detecting small and densely packed objects, owing to advances in multi-scale feature aggregation and attention-based refinement mechanisms that preserve fine-grained spatial details. Motivated by these strengths, we adopt YOLOv8 as our signboard detector. However, the INTSD comprises images captured under highly varying illumination conditions. While some scenes exhibit good lighting due to street lamps and vehicle headlights, others are severely underexposed in the absence of such sources. This variability poses a significant challenge for a static data pre-processing pipeline. To address this issue, we wrap the detector’s backbone with a *PreprocessWrapper* that applies a learned per-image parameter prediction head and differentiable transforms, producing preprocessed images which are then fed for detection.

**Param Head:** We introduce a small, convolutional parameter prediction head,  $\Phi_{\text{head}}$ , which takes a downsampled version of the normalized input image  $\mathbf{I}_{\text{norm}} \in \mathbb{R}^{H \times W \times 3}$  and predict raw parameter vector  $\mathbf{z}_{\text{raw}} \in \mathbb{R}^3$ .

$$\mathbf{z}_{\text{raw}} = \Phi_{\text{head}}(F_{\text{down}}(\mathbf{I}_{\text{norm}})) \quad (1)$$

where  $F_{\text{down}}$  is a bilinear resize operation to a fixed size.

This vector  $\mathbf{z}_{\text{raw}}$  is then scaled to produce three parameters:  $\gamma$  (gamma-correction amount),  $\alpha$  (brightness amount), and  $\zeta$  (unsharp mask amount). The scaling is achieved via a *tanh* activation to map the output to  $(-1, 1)$ , followed by a linear transformation to the parameter’s operational range ( $p$ ):

$$p = \frac{\tanh(z_i) + 1}{2}(p_{\text{max}} - p_{\text{min}}) + p_{\text{min}}, p \in \{\gamma, \alpha, \zeta\} \quad (2)$$

**Adaptive Image Enhancement:** The  $\mathbf{I}_{\text{norm}}$  is then transformed by this predicted set of parameters  $p$ . The differentiable transformation pipeline is given below:

1. **Unsharp Masking:** We first apply an unsharp mask to enhance edges. Mathematically,  $\mathbf{I}_U = \mathbf{I}_{\text{norm}} + \zeta \cdot (\mathbf{I}_{\text{norm}} - G_{\sigma_u}(\mathbf{I}_{\text{norm}}))$ , where  $G_{\sigma_u}$  is a Gaussian blur operation with a fixed kernel sigma  $\sigma_u$ .
2. **Gamma and Brightness Correction:** The  $\mathbf{I}_U$  is then corrected for contrast and brightness.  $\mathbf{I}_{\text{final}} = \text{clamp}(\alpha \cdot \text{clamp}(\mathbf{I}_U, \epsilon, 1.0)^\gamma, 0.0, 1.0)$ , where  $\epsilon$  is a small constant and *clamp* function is a standard mathematical operation, defined as:  $\text{clamp}(x, a, b) = \max(a, \min(x, b))$ . The inner clamp provides numerical stability for gradients, and outer clamp ensures a valid output data range.

To ensure that preprocessing module learns meaningful transformations and avoids collapsing to trivial solutions, we employ two key strategies. (i) *Stochastic Augmentation:* During training, we apply a diverse set of strong, non-differentiable augmentations (photometric jitter, JPEG compression, Gaussian noise, blur, and small rotations) before the image is passed to the *PreprocessWrapper*. It forces  $\Phi_{\text{head}}$  to learn to invert these degradations and normalize the image to a consistent domain for the detector. (ii) *Pre-processing Loss:* We apply an L2 regularization based loss ( $\mathcal{L}_{\text{preproc}}$ ) that penalizes the predicted scaled parameters for deviating from their (no operation) default values.

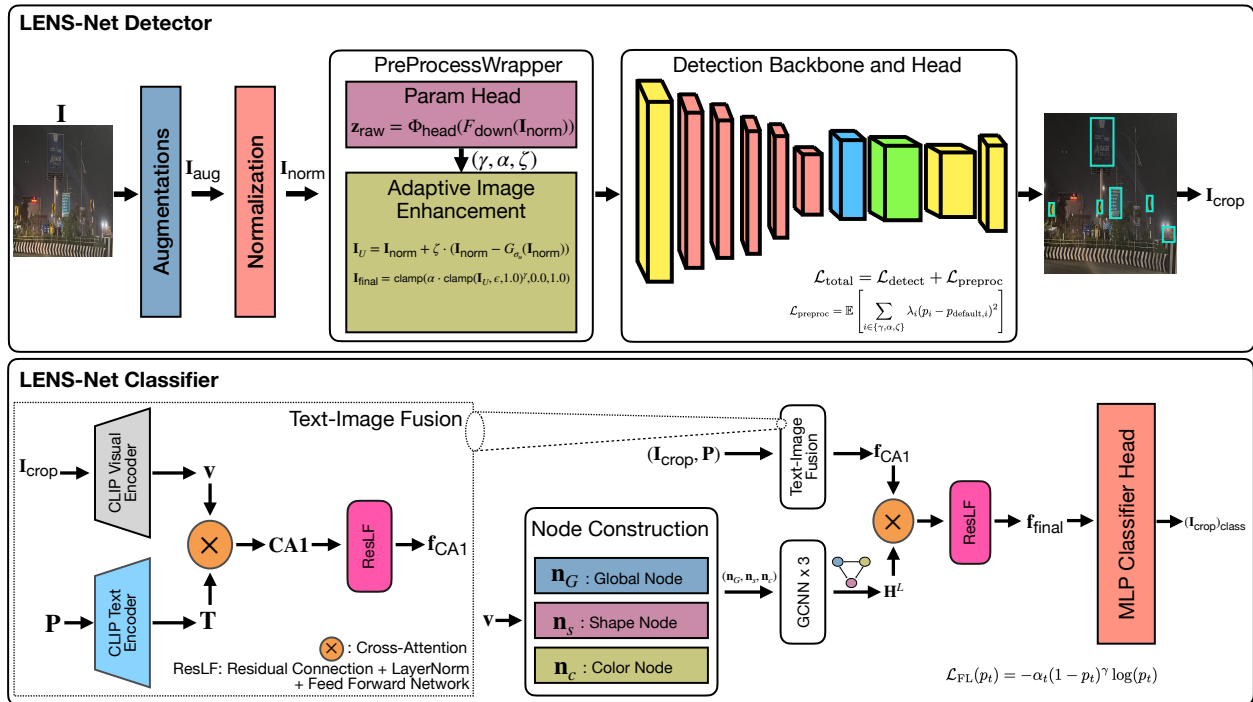


Figure 3. Overview of the proposed LENS-Net architecture. The LENS-Net detector (top) integrates adaptive image enhancement for joint illumination correction and sign localization. The LENS-Net classifier (bottom) employs a structured multimodal CLIP-GCNN module that leverages cross-modal attention and graph-based reasoning for sign classification.

$$\mathcal{L}_{\text{preproc}} = \mathbb{E} \left[ \sum_{i \in \{\gamma, \alpha, \zeta\}} \lambda_i (p_i - p_{\text{default}, i})^2 \right] \quad (3)$$

where  $\lambda_i$  ( $\lambda_i \in (0, 0.01)$ ) are per-parameter loss weights. This loss is added to the standard YOLOv8 detection loss,  $\mathcal{L}_{\text{detect}}$ , during training.

$$\mathcal{L}_{\text{total}} = \mathcal{L}_{\text{detect}} + \mathcal{L}_{\text{preproc}} \quad (4)$$

LENS-Net detector is trained using a zero-one scheduler: we first freeze the backbone and train  $\Phi_{\text{head}}$ , then unfreeze the backbone for joint end-to-end training. The detector’s bounding-box output ( $\mathbf{I}_{\text{crop}}$ ) is forwarded to the LENS-Net classifier, effectively filtering out the background, which does not contribute to TSR.

## 4.2. LENS-Net Classifier

After the detector localizes a traffic sign and outputs the corresponding cropped region, the classifier is tasked with accurately identifying the specific signboard category. We design a tri-modal fusion classifier that combines: (i) robust, global semantic features from a frozen CLIP vision encoder, (ii) prompt-conditioned textual priors from the CLIP text encoder, and (iii) structured attribute reasoning using a

small graph. The complete architecture is detailed in Algorithm 1. The model processes the  $\mathbf{I}_{\text{crop}}$  in two parallel branches that are fused for a final prediction.

**Branch 1: Text-Image Fusion.** We process  $\mathbf{I}_{\text{crop}}$  to obtain the corresponding global image embedding  $\mathbf{v}$ , which is fused with semantic context derived from a set of pre-defined textual prompts  $\mathbf{P}$ . These prompts are encoded into embeddings  $\mathbf{T} \in \mathbb{R}^{n(\mathbf{P}) \times D}$  using the frozen CLIP text encoder (Algorithm 1, line 2-3).  $\mathbf{v}$  serves as a holistic representation of the crop’s high-level visual semantics and  $\mathbf{T}$  is used for every image processed by the classifier, acting as a “semantic key/value store” that the model can attend to.

The L2 normalization of the image vector  $\mathbf{v}$  and all  $n(\mathbf{P})$  prompt vectors in  $\mathbf{T}$  projects them onto the surface of a  $D$ -dimensional unit hypersphere, allowing their dot product to be directly interpreted as cosine similarity. Normalization also ensures that the magnitude does not dominate the later computations.

We use a cross-attention module,  $\text{MHA}_{\text{CA1}}$  (Equation 5), where  $\mathbf{v}$  acts as the query ( $\mathbf{Q}$ ) and the text embeddings  $\mathbf{T}$  act as keys ( $\mathbf{K}$ ) and values ( $\mathbf{V}$ ). This produces a prompt-conditioned image feature  $\text{CA1}$ , a refined global vector that already blends visual information with textual priors.

$$\text{CA1} = \text{MHA}_{\text{CA1}}(\mathbf{Q} = \mathbf{v}, \mathbf{K} = \mathbf{T}, \mathbf{V} = \mathbf{T}) \quad (5)$$

---

**Algorithm 1** LENS-Net Classifier
 

---

**Require:** Image crop  $\mathbf{I}_{\text{crop}}$  (from LENS-Net Detector)

**Require:** Frozen  $E_{\text{clip}}^{\text{img}}, E_{\text{clip}}^{\text{text}}$ ; Static text prompts  $\mathbf{P}$   $\triangleright$  CLIP image and text encoders

**Ensure:** Class logits  $(\mathbf{I}_{\text{crop}})_{\text{class}}$

```

1: procedure CLASSIFIERFORWARD( $\mathbf{I}_{\text{crop}}$ )
  — Get Foundational Embeddings —
2:    $\mathbf{v} \leftarrow \text{L2Normalize}(E_{\text{clip}}^{\text{img}}(\mathbf{I}_{\text{crop}}))$   $\triangleright$  Image vector
3:    $\mathbf{T} \leftarrow \text{GetPrecomputedTextEmbeddings}(\mathbf{P})$   $\triangleright$  Prompt matrix
  — Branch 1: Text-Image Fusion —
4:    $\mathbf{f}_{\text{CA1}} \leftarrow \text{TextImageFusionModule}(\mathbf{v}, \mathbf{T})$   $\triangleright$  Handles  $\text{MHA}_{\text{CA1}}$ , Res, LN, FFN (Equation 6)
  — Branch 2: Graph Attribute Module —
5:    $\mathbf{H}^{(L)} \leftarrow \text{GraphAttributeModule}(\mathbf{v})$   $\triangleright$  Handles node creation & GCNN
  — Final Fusion & Classification —
6:    $\mathbf{f}_{\text{final}} \leftarrow \text{FinalFusionModule}(\mathbf{f}_{\text{CA1}}, \mathbf{H}^{(L)})$   $\triangleright$  Handles  $\text{MHA}_{\text{CA2}}$ , Res, LN, FFN (Equation 10)
7:    $(\mathbf{I}_{\text{crop}})_{\text{class}} \leftarrow \text{ClassifierHead}(\mathbf{f}_{\text{final}})$ 
8:   return  $(\mathbf{I}_{\text{crop}})_{\text{class}}$   $\triangleright$  Output class category
9: end procedure
10: function GraphAttributeModule( $\mathbf{v}$ )
11:    $\mathbf{n}_G \leftarrow \mathbf{v}$ 
12:    $\mathbf{n}_S \leftarrow (\text{Softmax}(\text{MLP}_S(\mathbf{v}))) \cdot \mathbf{E}_S$   $\triangleright \mathbf{E}_S$ : learnable shape embedding matrix
13:    $\mathbf{n}_C \leftarrow (\text{Softmax}(\text{MLP}_C(\mathbf{v}))) \cdot \mathbf{E}_C$   $\triangleright \mathbf{E}_C$ : learnable color embedding matrix
14:    $\mathbf{H}^{(0)} \leftarrow \text{Stack}(\mathbf{n}_G, \mathbf{n}_S, \mathbf{n}_C)$ 
15:    $\mathbf{H}^{(L)} \leftarrow \text{SimpleGCNN}(\mathbf{H}^{(0)})$ 
16:   return  $\mathbf{H}^{(L)}$ 
17: end function

```

---

The output  $\text{CA1}$  is processed through a residual connection (Res), Layer Normalization (LN), and position-wise feed-forward network (FFN) to get the text-fused image feature,  $\mathbf{f}_{\text{CA1}}$ , such that  $\mathbf{f}_{\text{CA1}} \in \mathbb{R}^D$ :

$$\mathbf{f}_{\text{CA1}} = \text{FFN}(\text{LN}(\mathbf{v} + \text{CA1})) \quad (6)$$

Equation 5 and 6 represents the *TextImageFusionModule* in Algorithm 1 (line 4).  $\mathbf{f}_{\text{CA1}}$  aligns the image’s representation with textual distinctions that are useful for traffic-sign recognition (e.g., color/shape descriptions, presence of numbers or arrows, etc.).

**Branch 2: Graph Attribute Module.** This branch explicitly models the two most salient attributes of signs: shape and color. As shown in the *GraphAttributeModule* (Algorithm 1, lines 10-17), we use the global image embedding  $\mathbf{v}$  to predict soft distributions over learnable shape ( $\mathbf{E}_S$ ) and color ( $\mathbf{E}_C$ ) embedding tables, turning the predicted distributions into continuous node vectors, i.e., instead of making a hard, non-differentiable *argmax* decision (e.g., this is 100% a circle), we represent uncertainty (e.g., [0.85 (circle), 0.1 (octagon), 0.05 (other)]).

For fine-grained sign classification, we identify three pillars of information as critical: the global appearance, the geometric shape, and the dominant color. Using these pillars, we construct a 3-node graph  $\mathbf{H}^{(0)}$ , composed of global appearance ( $\mathbf{n}_G = \mathbf{v}$ ), shape ( $\mathbf{n}_S$ ), and color ( $\mathbf{n}_C$ ) nodes.

These three nodes (all designed to live in the same  $D$ -dimensional embedding space) form a structured 3-node graph:  $\mathbf{H}^{(0)} = [\mathbf{n}_G, \mathbf{n}_S, \mathbf{n}_C]^T$ . We refer the interested readers to Appendix 9 for more details on node construction.

We use a 3-layer GCNN (*SimpleGCNN* on line 15 in Algorithm 1) operating on node matrix  $\mathbf{N}$  ( $\mathbf{N} = [\mathbf{n}_G, \mathbf{n}_S, \mathbf{n}_C], \mathbf{N} \in \mathbb{R}^{D \times 3}$ ). Let  $\mathbf{A} \in \mathbb{R}^{3 \times 3}$  be the fully-connected adjacency matrix (every node talks to every other). We normalize the adjacency matrix symmetrically (Equation 7) and perform a linear mapping followed by propagation with  $\hat{A}$  (Equation 8):

$$\hat{A} = D^{-\frac{1}{2}} \mathbf{A} D^{-\frac{1}{2}}, \quad D_{ii} = \sum_{j=1}^3 A_{ij}. \quad (7)$$

$$\mathbf{H}^{(l+1)} = \hat{A} (\mathbf{H}^{(l)} W^{(l)} + b^{(l)}), \quad \mathbf{H}^{(0)} = \mathbf{N}^T, \quad (8)$$

where  $\mathbf{H}^{(l)} \in \mathbb{R}^{3 \times D}$  is node features at layer  $l$ , and  $W^{(l)}, b^{(l)}$  are the layer parameters. After  $L$  layers, the GCNN outputs updated node features:  $\mathbf{H}^{(L)} \in \mathbb{R}^{3 \times D}$ .

The GCNN enables relational reasoning between nodes, i.e., if the  $\mathbf{n}_G$  suggests an arrow while the  $\mathbf{n}_S$  indicates an octagon, the GCNN mediates these signals to produce a joint representation capturing their agreement or conflict. Since the  $\mathbf{n}_G$  and  $\mathbf{n}_S$  originate from shared global embeddings, the GCNN effectively refines their features through message passing.

**Final Fusion.** After the GCNN, we fuse the two branches using a second cross-attention module,  $\text{MHA}_{\text{CA2}}$  (Algorithm 1, line 6). Here, the text-fused feature  $\mathbf{f}_{\text{CA1}}$  queries the GCNN-refined attribute nodes  $\mathbf{H}^{(L)}$  (Equation 9). This is a deliberate design choice: CA1 lets textual priors refine the image and CA2 lets the refined image go back and attend to structured attribute features. Conceptually, CA2 asks: “given what I now know from text, and given the shape/color-conditioned node features, how should I pool the node information to make final decision?” Mathematically,

$$\text{CA2} = \text{MHA}_{\text{CA2}}(\mathbf{Q} = \mathbf{f}_{\text{CA1}}, \mathbf{K} = \mathbf{H}^L, \mathbf{V} = \mathbf{H}^L) \quad (9)$$

This output is again processed with a residual connection, LN, and an FFN to produce the final, fully-fused feature vector  $\mathbf{f}_{\text{final}}$ :

$$\mathbf{f}_{\text{final}} = \text{FFN}(\text{LN}(\mathbf{f}_{\text{CA1}} + \text{CA2})) \quad (10)$$

The final vector  $\mathbf{f}_{\text{final}}$  (Equation 10) is passed to an MLP head (Algorithm 1, line 7) and produces logits  $((\mathbf{I}_{\text{crop}})_{\text{class}} \in \mathbb{R}^N)$  over the target traffic-sign classes.

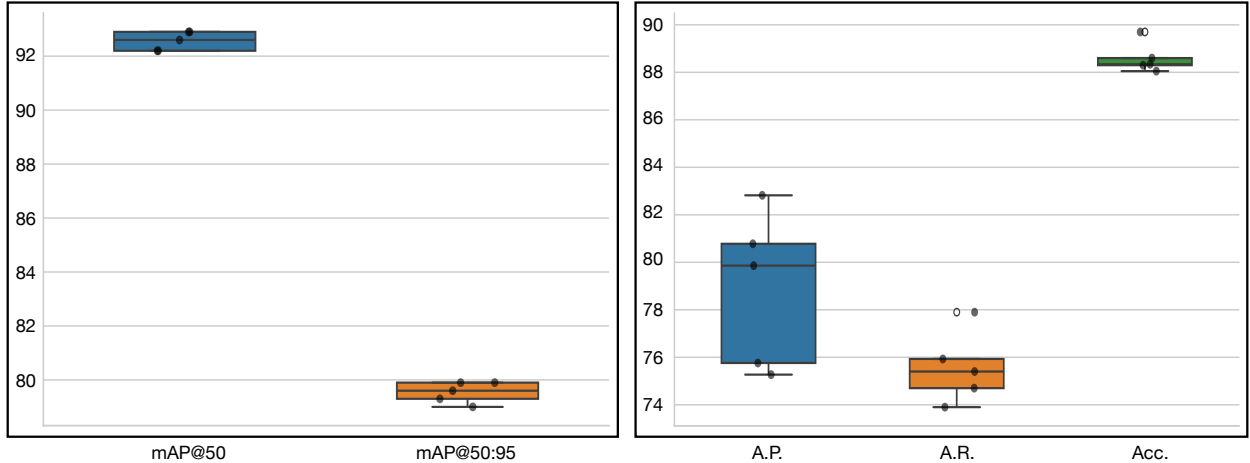


Figure 4. Fold-wise performance of LENS-Net for detection (left) and classification (right) on INTSD. A.P., A.R. and Acc. denotes macro-averaged precision, macro-averaged recall and accuracy, respectively.

**Classifier Training Objective.** The LENS-Net classifier is trained using the focal loss [26] that includes per-class weights computed from training frequencies (rarer classes get larger weights to reduce bias toward common classes). This is done to address the significant class imbalance inherent in INTSD.

$$\mathcal{L}_{\text{FL}}(p_t) = -\alpha_t(1 - p_t)^\gamma \log(p_t) \quad (11)$$

where  $p_t$  is the model’s predicted probability for the ground-truth class, and  $\gamma$  is the focusing parameter. We further employ a class-balancing variant where  $\alpha_t$  is the inverse square root of the class frequency, normalized to sum to  $N$ .

$$\alpha_t = \frac{1/\sqrt{\text{count}(t)}}{\sum_{j=1}^N (1/\sqrt{\text{count}(j)})} \times N \quad (12)$$

To further mitigate imbalance, we employ a rarity-based augmentation (mentioned in Appendix 9). Implementation details are given in Appendix 8.

## 5. Results

**Experimental Settings.** We adopt a stratified 5-fold cross-validation strategy for training and evaluation. We choose mAP@50 and mAP@50:95 as detection evaluation metrics and macro-averaged precision (A.P.), macro-averaged recall (A.R.), and accuracy (Acc.) as classification evaluation metrics.

**Baseline Results.** In Tables 2 and 3, we show strong baselines and benchmark INTSD for detection and classification, respectively. We demonstrate experimental results using: (i) DAI-Net [7], (ii) Faster R-CNN [39] with Feature Pyramid Network (FPN) [21] and residual networks (ResNet) [17] as their backbone, (iii) YOLOv8 [38], (iv)

Table 2. Detection performance on the INTSD.

Model	mAP@50 (%)	mAP@50:95 (%)
Faster R-CNN [39]	62.60	43.22
DAI-Net [7]	87.18	62.56
YOLOv8 [38]	90.13	77.21
YOLO-TS [3]	90.77	77.27
<b>LENS-Net</b>	<b>92.56</b>	<b>79.54</b>

YOLO-TS [3], (v) BLIP [23], (v) CLIP [36], (vi) DeiT [47] and Rishabh et al. [50].

**Detection.** Table 2 summarizes the detection performance on the INTSD dataset. The proposed LENS-Net detector achieves the highest accuracy among all compared methods, substantially outperforming Faster R-CNN [39] and DAI-Net [7]. While YOLOv8 [38] and YOLO-TS [3] show comparable results, both lag behind LENS-Net, confirming the benefit of our adaptive enhancement and the effectiveness of our detector in handling diverse and challenging traffic sign instances.

Figure 4 (left) shows the 5-fold performance of the LENS-Net detector. The scores are tightly clustered around 92.5% mAP@50, indicating strong and consistent detection ability. The smaller mAP@50:95 values suggest slightly lower precision in tight localization, though the low variance demonstrates overall stability.

**Classification.** Table 3 presents the classification results on INTSD. LENS-Net achieves the best performance across all metrics, outperforming the previous state-of-the-art by Rishabh et al. [50] by **+8.4%** in A.P. and **+8.57%** in A.R. It also yields the highest accuracy of **88.59%**, highlighting the strength of its multimodal fusion and attribute-guided reasoning.

LENS-Net classifier shows consistently high accuracy



Figure 5. Qualitative results of LENS-Net on INTSD. The green, red, and blue boxes indicate true positives, false negatives, and false positives, respectively. The numbers on the boxes represent the corresponding class IDs.

Table 3. Classification results on the INTSD.

Model	A.P. (%)	A.R. (%)	Acc. (%)
BLIP [23]	49.33	47.81	69.90
CLIP [36]	65.25	68.11	82.49
DeIT [47]	65.89	59.69	82.13
Rishabh et al. [50]	70.49	66.99	85.21
<b>LENS-Net</b>	<b>78.89</b>	<b>75.56</b>	<b>88.59</b>

(Figure 4, right), with scores tightly clustered around 88.5%, indicating stability across folds. In contrast, A.P. and A.R. show lower medians ( $\approx 79.5\%$  and  $75.5\%$ ) and higher variance, suggesting less consistency in handling per-class precision-recall performance. Figure 5 gives the predictions of LENS-Net on INTSD along with false positives and false negatives.

**Ablation Study.** Figure 6 depicts the contribution of key components in LENS-Net. Removing the *GraphAttributeModule* causes a 3.92% and 3.36% drop in A.P. and A.R., confirming that the GCNN effectively models relational dependencies among global, shape, and color nodes through message passing, enabling compositional reasoning (e.g., “red octagon  $\rightarrow$  stop sign”).

Replacing cross-attention fusion (*TextImageFusionModule* and *FinalFusionModule*) with simple concatenation reduces A.P. and A.R. by 5.0% and 3.18%, validating that cross-attention is crucial for meaningful multimodal interaction among image, text, and graph features. Similarly, ablating text prompts (**P**) leads to a 2.21% and 1.84% drop, showing their role as text-guided priors that inject semantic knowledge of sign attributes and leverage CLIP’s vision-language alignment to resolve visually similar classes.

Eliminating the learned shape ( $\mathbf{E}_S$ ) and color ( $\mathbf{E}_C$ ) embedding tables and using simple projections ( $MLP_S(\mathbf{v})$  and  $MLP_C(\mathbf{v})$ ) results in 3.8% and 1.86% drops in A.P. and A.R. These embeddings allow the model to learn semantically rich geometric and chromatic representations within the CLIP feature space.

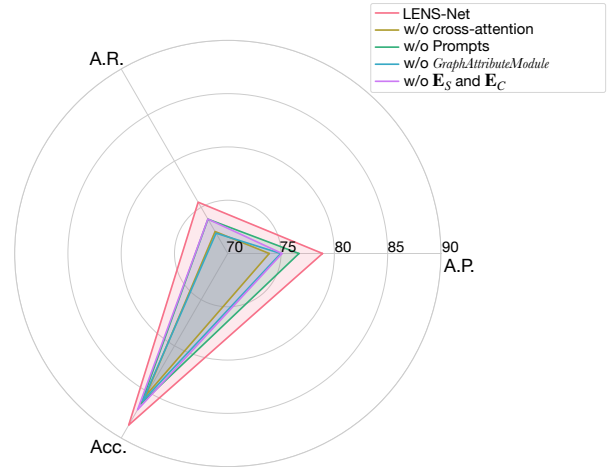


Figure 6. Ablation study on the impact of major components in LENS-Net for traffic sign classification on INTSD.

## 6. Conclusion

We present INTSD, the first nighttime dataset for traffic sign detection and classification, and LENS-Net, a multimodal framework that unifies adaptive enhancement, vision-language priors, and graph-based reasoning. Experimental results demonstrate LENS-Net’s superior performance, providing a valuable benchmark and foundation for future research on robust perception in adverse illumination environments.

## References

- [1] Dongliang Chang, Yujun Tong, Ruoyi Du, Timothy Hospedales, Yi-Zhe Song, and Zhanyu Ma. An erudite fine-grained visual classification model. In *Proceedings of the IEEE/CVF Conference on Computer Vision and Pattern Recognition*, pages 7268–7277, 2023. 2
- [2] Chen Chen, Qifeng Chen, Jia Xu, and Vladlen Koltun. Learning to see in the dark. In *Proceedings of the IEEE conference on computer vision and pattern recognition*, pages 3291–3300, 2018. 1
- [3] Junzhou Chen, Heqiang Huang, Ronghui Zhang, Nengchao Lyu, Yanyong Guo, Hong-Ning Dai, and Hong Yan. Yolo-ts: Real-time traffic sign detection with enhanced accuracy us-

- ing optimized receptive fields and anchor-free fusion. *IEEE Transactions on Intelligent Transportation Systems*, 2025. 7
- [4] Ziteng Cui, Kunchang Li, Lin Gu, Shenghan Su, Peng Gao, Zhengkai Jiang, Yu Qiao, and Tatsuya Harada. You only need 90k parameters to adapt light: a light weight transformer for image enhancement and exposure correction. *arXiv preprint arXiv:2205.14871*, 2022. 2
- [5] Saba Dadsetan, David Pichler, David Wilson, Naira Hovakimyan, and Jennifer Hobbs. Superpixels and graph convolutional neural networks for efficient detection of nutrient deficiency stress from aerial imagery. In *Proceedings of the IEEE/CVF Conference on Computer Vision and Pattern Recognition*, pages 2950–2959, 2021. 2
- [6] Jifeng Dai, Yi Li, Kaiming He, and Jian Sun. R-fcn: Object detection via region-based fully convolutional networks. *Advances in neural information processing systems*, 29, 2016. 2
- [7] Zhipeng Du, Miaoqing Shi, and Jiankang Deng. Boosting object detection with zero-shot day-night domain adaptation. In *Proceedings of the IEEE/CVF Conference on Computer Vision and Pattern Recognition*, pages 12666–12676, 2024. 7
- [8] Abhishek Dutta and Andrew Zisserman. The via annotation software for images, audio and video. In *Proceedings of the 27th ACM international conference on multimedia*, pages 2276–2279, 2019. 3
- [9] Christian Ertler, Jerneja Mislej, Tobias Ollmann, Lorenzo Porzi, Gerhard Neuhold, and Yubin Kuang. The mapillary traffic sign dataset for detection and classification on a global scale. In *European conference on computer vision*, pages 68–84. Springer, 2020. 1, 2, 3
- [10] Mark Everingham, SM Ali Eslami, Luc Van Gool, Christopher KI Williams, John Winn, and Andrew Zisserman. The pascal visual object classes challenge: A retrospective. *International journal of computer vision*, 111(1):98–136, 2015. 1
- [11] Kevin Eykholt, Ivan Evtimov, Earlene Fernandes, Bo Li, Amir Rahmati, Chaowei Xiao, Atul Prakash, Tadayoshi Kohno, and Dawn Song. Robust physical-world attacks on deep learning visual classification. In *Proceedings of the IEEE conference on computer vision and pattern recognition*, pages 1625–1634, 2018. 1
- [12] Ali Farzipour, Omid Nejati Manzari, and Shahriar B Shokouhi. Traffic sign recognition using local vision transformer. In *2023 13th International Conference on Computer and Knowledge Engineering (ICCKE)*, pages 191–196. IEEE, 2023. 2
- [13] Ross Girshick, Jeff Donahue, Trevor Darrell, and Jitendra Malik. Rich feature hierarchies for accurate object detection and semantic segmentation. In *Proceedings of the IEEE conference on computer vision and pattern recognition*, pages 580–587, 2014. 2
- [14] Chunle Guo, Chongyi Li, Jichang Guo, Chen Change Loy, Junhui Hou, Sam Kwong, and Runmin Cong. Zero-reference deep curve estimation for low-light image enhancement. In *Proceedings of the IEEE/CVF conference on computer vision and pattern recognition*, pages 1780–1789, 2020. 2
- [15] Mrinal Haloi. Traffic sign classification using deep inception based convolutional networks. *arXiv preprint arXiv:1511.02992*, 2015. 2
- [16] Yan Han and Erdal Oruklu. Traffic sign recognition based on the nvidia jetson tx1 embedded system using convolutional neural networks. In *2017 IEEE 60th International Midwest Symposium on Circuits and Systems (MWSCAS)*, pages 184–187. IEEE, 2017. 2
- [17] Kaiming He, Xiangyu Zhang, Shaoqing Ren, and Jian Sun. Deep residual learning for image recognition. In *Proceedings of the IEEE conference on computer vision and pattern recognition*, pages 770–778, 2016. 7
- [18] Judy Hoffman, Eric Tzeng, Taesung Park, Jun-Yan Zhu, Phillip Isola, Kate Saenko, Alexei Efros, and Trevor Darrell. Cycada: Cycle-consistent adversarial domain adaptation. In *International conference on machine learning*, pages 1989–1998. Pmlr, 2018. 1
- [19] Alex Krizhevsky, Ilya Sutskever, and Geoffrey E Hinton. Imagenet classification with deep convolutional neural networks. *Advances in neural information processing systems*, 25, 2012. 1
- [20] Alina Kuznetsova, Hassan Rom, Neil Alldrin, Jasper Uijlings, Ivan Krasin, Jordi Pont-Tuset, Shahab Kamali, Stefan Popov, Matteo Mallocci, Alexander Kolesnikov, et al. The open images dataset v4: Unified image classification, object detection, and visual relationship detection at scale. *International journal of computer vision*, 128(7):1956–1981, 2020. 1
- [21] Fredrik Larsson and Michael Felsberg. Using fourier descriptors and spatial models for traffic sign recognition. In *Scandinavian conference on image analysis*, pages 238–249. Springer, 2011. 2, 7
- [22] Jianan Li, Xiaodan Liang, Yunchao Wei, Tingfa Xu, Jiashi Feng, and Shuicheng Yan. Perceptual generative adversarial networks for small object detection. In *Proceedings of the IEEE conference on computer vision and pattern recognition*, pages 1222–1230, 2017. 1
- [23] Junnan Li, Dongxu Li, Caiming Xiong, and Steven Hoi. Blip: Bootstrapping language-image pre-training for unified vision-language understanding and generation. In *International conference on machine learning*, pages 12888–12900. PMLR, 2022. 7, 8
- [24] Tsung-Yi Lin, Michael Maire, Serge Belongie, James Hays, Pietro Perona, Deva Ramanan, Piotr Dollár, and C Lawrence Zitnick. Microsoft coco: Common objects in context. In *European conference on computer vision*, pages 740–755. Springer, 2014. 1
- [25] Tsung-Yi Lin, Piotr Dollár, Ross Girshick, Kaiming He, Bharath Hariharan, and Serge Belongie. Feature pyramid networks for object detection. In *Proceedings of the IEEE conference on computer vision and pattern recognition*, pages 2117–2125, 2017. 2
- [26] Tsung-Yi Lin, Priya Goyal, Ross Girshick, Kaiming He, and Piotr Dollár. Focal loss for dense object detection. In *Proceedings of the IEEE international conference on computer vision*, pages 2980–2988, 2017. 2, 7
- [27] Ziyu Lin, Yunfan Wu, Yuhang Ma, Junzhou Chen, Ronghui Zhang, Jiaming Wu, Guodong Yin, and Liang Lin. Yolo-llts:

- Real-time low-light traffic sign detection via prior-guided enhancement and multi-branch feature interaction. *arXiv preprint arXiv:2503.13883*, 2025. 1
- [28] Wei Liu, Dragomir Anguelov, Dumitru Erhan, Christian Szegedy, Scott Reed, Cheng-Yang Fu, and Alexander C Berg. Ssd: Single shot multibox detector. In *European conference on computer vision*, pages 21–37. Springer, 2016. 1, 2
- [29] Wenyu Liu, Gaofeng Ren, Runsheng Yu, Shi Guo, Jianke Zhu, and Lei Zhang. Image-adaptive yolo for object detection in adverse weather conditions. In *Proceedings of the AAAI conference on artificial intelligence*, pages 1792–1800, 2022. 2
- [30] Chengsheng Mao, Liang Yao, and Yuan Luo. Imagegcnn: Multi-relational image graph convolutional networks for disease identification with chest x-rays. *IEEE transactions on medical imaging*, 41(8):1990–2003, 2022. 2
- [31] Markus Mathias, Radu Timofte, Rodrigo Benenson, and Luc Van Gool. Traffic sign recognition—how far are we from the solution? In *The 2013 international joint conference on Neural networks (IJCNN)*, pages 1–8. IEEE, 2013. 2
- [32] Aditya Mishra, Ahnaf Mozib Samin, Ali Etemad, and Javad Hashemi. Subject representation learning from eeg using graph convolutional variational autoencoders. In *ICASSP 2025-2025 IEEE International Conference on Acoustics, Speech and Signal Processing (ICASSP)*, pages 1–5. IEEE, 2025. 2
- [33] Andreas Mogelmose, Mohan Manubhai Trivedi, and Thomas B Moeslund. Vision-based traffic sign detection and analysis for intelligent driver assistance systems: Perspectives and survey. *IEEE transactions on intelligent transportation systems*, 13(4):1484–1497, 2012. 2
- [34] Gerhard Neuhold, Tobias Ollmann, Samuel Rota Buló, and Peter Kotschieder. The mapillary vistas dataset for semantic understanding of street scenes. In *Proceedings of the IEEE international conference on computer vision*, pages 4990–4999, 2017. 2
- [35] Abhijith Punnappurath, Abdullah Abuolaim, Abdelrahman Abdelhamed, Alex Levinshtein, and Michael S Brown. Day-to-night image synthesis for training nighttime neural nets. In *Proceedings of the IEEE/CVF Conference on Computer Vision and Pattern Recognition*, pages 10769–10778, 2022. 1
- [36] Alec Radford, Jong Wook Kim, Chris Hallacy, Aditya Ramesh, Gabriel Goh, Sandhini Agarwal, Girish Sastry, Amanda Askell, Pamela Mishkin, Jack Clark, et al. Learning transferable visual models from natural language supervision. In *International conference on machine learning*, pages 8748–8763. PmLR, 2021. 2, 7, 8
- [37] Joseph Redmon and Ali Farhadi. Yolo9000: better, faster, stronger. In *Proceedings of the IEEE conference on computer vision and pattern recognition*, pages 7263–7271, 2017. 2
- [38] Joseph Redmon, Santosh Divvala, Ross Girshick, and Ali Farhadi. You only look once: Unified, real-time object detection. In *Proceedings of the IEEE conference on computer vision and pattern recognition*, pages 779–788, 2016. 1, 7
- [39] Shaoqing Ren, Kaiming He, Ross Girshick, and Jian Sun. Faster r-cnn: Towards real-time object detection with region proposal networks. *Advances in neural information processing systems*, 28, 2015. 1, 2, 7
- [40] J Rodrigues and J Carbonera. Graph convolutional networks for image classification: Comparing approaches for building graphs from images. In *Proceedings of the 26th International Conference on Enterprise Information Systems-Volume 1: ICEIS*, pages 437–446, 2024. 2
- [41] Christos Sakaridis, Dengxin Dai, and Luc Van Gool. Acdd: The adverse conditions dataset with correspondences for semantic driving scene understanding. In *Proceedings of the IEEE/CVF international conference on computer vision*, pages 10765–10775, 2021. 1
- [42] Vladislav Igorevich Shakhuro and Anton Sergeevich Konushin. Russian traffic sign images dataset. *Computer optics*, 40(2):294–300, 2016. 1, 2
- [43] Johannes Stallkamp, Marc Schlipsing, Jan Salmen, and Christian Igel. The german traffic sign recognition benchmark: a multi-class classification competition. In *The 2011 international joint conference on neural networks*, pages 1453–1460. IEEE, 2011. 2
- [44] Johannes Stallkamp, Marc Schlipsing, Jan Salmen, and Christian Igel. Man vs. computer: Benchmarking machine learning algorithms for traffic sign recognition. *Neural networks*, 32:323–332, 2012. 2
- [45] Xiaoqiang Sun, Kuankuan Liu, Long Chen, Yingfeng Cai, and Hai Wang. Llth-yolov5: a real-time traffic sign detection algorithm for low-light scenes. *Automotive Innovation*, 7(1): 121–137, 2024. 1, 2
- [46] Ying Sun, Pingshu Ge, and Dequan Liu. Traffic sign detection and recognition based on convolutional neural network. In *2019 Chinese automation congress (CAC)*, pages 2851–2854. IEEE, 2019. 2
- [47] Hugo Touvron, Matthieu Cord, Matthijs Douze, Francisco Massa, Alexandre Sablayrolles, and Hervé Jégou. Training data-efficient image transformers & distillation through attention. In *International conference on machine learning*, pages 10347–10357. PMLR, 2021. 7, 8
- [48] Dai Quoc Tran, Armstrong Aboah, Yuntae Jeon, Maged Shoman, Minsoo Park, and Seunghee Park. Low-light image enhancement framework for improved object detection in fisheye lens datasets. In *Proceedings of the IEEE/CVF Conference on Computer Vision and Pattern Recognition (CVPR) Workshops*, pages 7056–7065, 2024. 2
- [49] Vivek Trivedy and Longin Jan Latecki. Cnn2graph: Building graphs for image classification. In *Proceedings of the IEEE/CVF Winter Conference on Applications of Computer Vision*, pages 1–11, 2023. 2
- [50] Rishabh Uikey, Haroon R Lone, and Akshay Agarwal. Indian traffic sign detection and classification through a unified framework. *IEEE Transactions on Intelligent Transportation Systems*, 25(10):14866–14875, 2024. 3, 7, 8, 6
- [51] Ze Yang, Tiange Luo, Dong Wang, Zhiqiang Hu, Jun Gao, and Liwei Wang. Learning to navigate for fine-grained classification. In *Proceedings of the European conference on computer vision (ECCV)*, pages 420–435, 2018. 2
- [52] Fisher Yu, Wenqi Xian, Yingying Chen, Fangchen Liu, Mike Liao, Vashisht Madhavan, Trevor Darrell, et al. Bdd100k: A

diverse driving video database with scalable annotation tooling. *arXiv preprint arXiv:1805.04687*, 2(5):6, 2018. [2](#)

- [53] Jun-Yan Zhu, Taesung Park, Phillip Isola, and Alexei A Efros. Unpaired image-to-image translation using cycle-consistent adversarial networks. In *Proceedings of the IEEE international conference on computer vision*, pages 2223–2232, 2017. [1](#)
- [54] Zhe Zhu, Dun Liang, Songhai Zhang, Xiaolei Huang, Baoli Li, and Shimin Hu. Traffic-sign detection and classification in the wild. In *Proceedings of the IEEE conference on computer vision and pattern recognition*, pages 2110–2118, 2016. [1](#), [2](#)

# Navigating in the Dark: A Multimodal Framework and Dataset for Nighttime Traffic Sign Recognition

## Supplementary Material

### 7. Indian Nighttime Traffic Sign Dataset

This section provides representative examples from our dataset, illustrating the various challenges, supplementary classes, weather conditions, and daytime scenarios detailed in Section 3. A summary of all figures is given in Table 4.

Table 4. Summary of all the figures.

Figure	Description
Figure 7	Sensor and weather differences
Figure 8	Different challenges in INTSD
Figure 9	Motion Blur
Figure 10	Glare
Figure 11	Low-illumination
Figure 12	Multiple signboards
Figure 13	Intra-class variability
Figure 14	<i>tampered</i> class
Figure 15	<i>unknown</i> class
Figure 16	<i>warning</i> class
Figure 17	<i>advertisement</i> class
Figure 18	Day images in INTSD

**Examples:** Figure 7 illustrates representative samples from our dataset. The top-left and bottom-left images were captured using a smartphone, whereas the top-right and bottom-right images were acquired using an action camera. The quality gap between the two sensor types is clearly visible. Additionally, the top row shows images captured under normal weather conditions, while the bottom row depicts images taken during rainfall. As shown, rain significantly degrades image quality and introduces substantial noise, making traffic sign detection more challenging. The figure also showcases the quality difference between images collected from smartphones and action cameras.

**Challenges:** Figure 8 illustrates several of the challenges discussed in Section 3. Specifically, the figure shows:

- Top left: sign partially occluded by foliage;
- Top right: traffic sign obscured by other signs;
- Bottom left: signs that are partially out of frame;
- Bottom right: signs that form part of larger signboards.

Apart from the challenges discussed above, INTSD contains several additional forms of visual noise that hinder reliable signboard detection and classification. The vehicle-mounted camera setup inherently introduces motion blur into the recordings – a natural outcome of vehicle motion and road-induced vibrations. This adds an additional layer of difficulty for downstream detection and classifica-



Figure 7. Examples of dataset images from smartphone (left) and action camera (right) under normal (top) and rainy (bottom) weather conditions.



Figure 8. Illustration of selected challenges within the INTSD, with problematic signboards highlighted in red to clearly differentiate them from the remaining elements. The images are captured from smartphones.

tion tasks. Figure 9 illustrates motion blur caused by vehicle movement, while Figure 10 shows examples of headlight and street-light glare that further degrade image clarity. Figure 11 presents samples captured in poorly lit environments; such low-illumination conditions significantly complicate detection and highlight the need for robust and adaptive image-enhancement techniques prior to downstream tasks.

Indian roads are often visually complex. Figure 12 de-

picts scenes containing multiple signboards within a single frame and Figure 13 illustrates different signboard designs conveying the same meaning. These variations introduce additional ambiguity and increase the difficulty of accurate signboard recognition.



Figure 9. Examples of motion blur caused by vehicle movement, reducing signboard visibility. The image on left has been captured from action camera and the image on right has been acquired from smartphone.



Figure 10. Samples showing headlight and street-light glare that obscures signboard details. The images on left and right were gathered from smartphone and action camera, respectively.



Figure 11. Images captured under low-light conditions, illustrating the difficulty of detecting signs in dark environments. Both images have been captured from action camera.

**Additional Classes:** The four supplementary classes that are misclassified by TSR models and are absent in existing benchmarks are shown in Figures 14, 15, 16, and 17.

**Additional Day Images:** We also include additional daytime images in the dataset, with examples shown in Figure 18. The top-row samples, captured using smartphones, generally exhibit higher visual quality compared to the bottom-row images captured with an action camera.



Figure 12. Images with multiple signboards in one frame, creating the kind of visual clutter common on Indian roads. Both images have been taken from smartphone.



Figure 13. Four distinct signboard designs, all conveying mapping to *school* class, highlighting intra-class appearance variation. The images on top are from smartphone and that on bottom are from action camera.



Figure 14. Representative examples of the *tampered* class in the INTSD. All the images are captured from smartphone.

In summary, the INTSD offers a comprehensive and realistically challenging benchmark for nighttime traffic sign recognition, an area largely underrepresented in existing



Figure 15. Illustrative samples of images labeled as *unknown* within the INTSD. The image on bottom right has been acquired from action camera and the remaining are from smartphone.



Figure 17. Visual examples demonstrating the *advertisement* class within INTSD. The image on top right has been taken from smartphone and the remaining from action camera.



Figure 16. Sample instances of the *warning* category from INTSD. All the images have been obtained from smartphone.



Figure 18. Sample instances of the day images from INTSD. The images on top are captured from smartphone and those on bottom are from action camera.

datasets. Its diverse collection of sensor qualities, weather conditions, illumination levels, intra-class variations, and real-world visual noise captures the complexity of Indian road environments with high fidelity. Beyond traffic sign recognition, the dataset provides valuable opportunities for research in broader computer vision tasks, including general object detection and classification, low-to-high-quality image translation, and day-to-night or night-to-day domain adaptation. By encompassing such a wide spectrum of real-world conditions, INTSD serves as a robust platform for developing resilient perception models for autonomous driving and related applications.

## 8. Implementation Details

This section provides the implementation details for both components of our pipeline: (i) LENS-Net detector, and (ii) LENS-Net classifier. All hyperparameters and training settings reported here correspond to those used in our study. We used a system with a 16 GB NVIDIA GeForce RTX 5080 to train the model. The LENS-Net detector and classifier have 11.13M and 11.75M parameters (excluding frozen CLIP parameters), respectively.

### 8.1. LENS-Net Detector

We build upon the Ultralytics YOLO architecture and wrap the detector with a lightweight *PreProcessWrapper* module that predicts per-image enhancement parameters before

feeding images to the detection backbone. The wrapper includes a small CNN (three stride-2 convolutional layers followed by an MLP) that outputs three parameters:

- gamma correction ( $\gamma$ )
- brightness scaling ( $\alpha$ )
- sharpening amount ( $\zeta$ )

These parameters are mapped to natural ranges, i.e.,  $\gamma \in [0.3, 3.0]$ ,  $\alpha \in [0.3, 4.0]$ , and  $\zeta \in [0, 1.2]$ , and are applied using differentiable operations. A small regularization loss (Equation 3) keeps parameters close to their no operation values ( $\mathbf{p}_{\text{default}} = [\gamma = 1.0, \alpha = 1.0, \zeta = 0.0]$ ) to avoid over-enhancement.

**Augmentations.** We apply probabilistic image augmentations during training, including photometric jitter, JPEG compression, Gaussian noise, blur, and  $\pm 5^\circ$  rotation. Each augmentation family has a type weight given by Table 5.

Table 5. Weights associated with each type of augmentation during detection phase.

Augmentation	Weight
Photometric	1.0
JPEG	0.9
Gaussian	0.8
Blur	0.6
Rotation	0.5

After selecting an augmentation family, the final probability of applying it to an image is computed as:

$$\mathbf{p}_{\text{aug}} = \text{clamp}(\mathbf{p}_{\text{class}} \cdot \mathbf{w}_{\text{type}}, 0.05, 0.95) \quad (13)$$

where  $\mathbf{p}_{\text{class}}$  is the probability that a sample from a particular class will be augmented and its calculation is given in Appendix 9, and  $\mathbf{w}_{\text{type}}$  is the corresponding type weight from Table 5. The clamping ensures that every augmentation has a minimum probability of 0.05 and cannot exceed 0.95, preventing both under-augmentation and over-augmentation. This formulation enables augmentation intensity to adapt naturally to the relative severity of each transformation while maintaining stable training dynamics.

The rest of the hyperparameters and their values used in the LENS-Net detector are given in Table 6.

## 8.2. LENS-Net Classifier

We use a Tri-Modal Fusion classifier consisting of: (i) CLIP image embeddings (frozen ViT-L/14 backbone), (ii) CLIP text prompt embeddings (5 prompts), and (iii) Shape and color embeddings predicted from small MLP heads. These three sources form a 3-node graph which is processed by a GCNN, followed by a second fusion module

Table 6. List of all the hyperparameters used in LENS-Net detector. The list encompasses values used by detector backbone and *PreProcWrapper* (in order).  $\dagger$  represents the downsampled image size that is passed to *PreProcWrapper*.

Hyperparameter	Value
Backbone Weights	<i>yolov8s.pt</i>
Image Size	640
Batch Size	32
Workers	8
Head Epochs ( $\mathbf{E}_{\text{head}}$ )	10
Joint Epochs ( $\mathbf{E}_{\text{joint}}$ )	50
Preproc Downsample $\dagger$	64
$\lambda_\gamma$	0.001
$\lambda_\alpha$	0.001
$\lambda_\zeta$	0.005

Table 7. List of all the hyperparameters used in LENS-Net classifier. The list encompasses values used during data loading and caching, and training (in order).

Hyperparameter	Value
Batch Size	64
Workers	4
Pin Memory	True
Persistent Workers	True
Prefetch Factor	2
Multiprocessing	spawn
Context	
Epochs	50
Batch Size	64
Learning Rate	$1 \times 10^{-4}$
Weight Decay	$1 \times 10^{-5}$
Dropout	0.2
Workers	4
$\gamma_{\text{focal}}$	2.0
Prefetch Factor	2
Image Size	224
$\mathbf{p}_{\text{base}}$	0.15
$\mathbf{p}_{\text{scale}}$	0.75
Shape Categories	<i>circle, rectangle, octagon, triangle</i>
Color Categories	<i>red, blue, green, yellow, white, black, other</i>
CLIP Model	<i>clip-vit-large-patch14</i>

and a classification head.

**Data Handling.** Images are loaded per class directory. During training, augmentations are applied at the PIL (Python Imaging Library) level.

We report the key PyTorch *DataLoader* parameters used throughout our experiments for both training and evaluation. Several of these settings are hardware-aware: *pin\_memory* is enabled when using CUDA to accelerate host-to-device transfers, while *persistent\_workers* is acti-

vated when the number of workers is greater than zero to avoid worker re-initialization overhead across epochs. We keep the default *prefetch\_factor* of 2, which controls how many batches each worker prepares in advance, improving input pipeline throughput. In addition, we explicitly set the multiprocessing context to “spawn” to ensure stable worker initialization across platforms and avoid fork-related issues when loading large models. These configuration choices collectively improve data-loading efficiency without altering the model’s learning dynamics.

**Prompts.** We use the following set of 5 predefined prompts to generate the textual embedding  $\mathbf{T}$  using frozen CLIP text encoder:

1. *Describe the traffic sign in detail, including any visible text or numbers.*
2. *What is the color and geometric shape of the sign and what does it convey (warning, mandatory, prohibition, information)?*
3. *Is there an icon or pictogram? Describe the icon (car, truck, pedestrian, arrow, fuel pump, etc.).*
4. *Extract any text, numbers or symbols from the sign and list them.*
5. *Is this sign an advertisement, a regulatory sign, a warning sign, or an informational sign? If none apply or the image is unreadable/occluded, reply 'unclassifiable'. Keep your answer one word.*

**Loss and Class Imbalance.** We use focal loss with  $\gamma_{\text{focal}} = 2.0$ . Per-class  $\alpha_t$  weights (Equation 12) are computed inversely proportional to the square root of frequency. Table 7 lists all the hyperparameters and their values used in the LENS-Net classifier.

**Data Splits.** We adopt a stratified 5-fold cross-validation strategy for training and evaluation. This ensures that each fold has a balanced representation of all classes. Specifically, the dataset splits consist of 1188, 1226, 1175, 1189 and 1226 images with 2133, 2134, 2129, 2133 and 2128 signboard instances, respectively. These standardized splits have been released publicly, along with the dataset to facilitate fair comparisons and benchmarking by future researchers, promoting reproducibility and consistent evaluation across studies.

## 9. Method

We provide the complete architecture of the LENS-Net detector in Algorithm 2. For a given image crop  $\mathbf{I}_{\text{crop}}$  from the LENS-Net detector, we pass it through the frozen CLIP Vision Transformer (ViT). We extract the output embedding from the CLIP image encoder ( $E_{\text{clip}}^{\text{img}}$ ), yielding an L2-normalized global feature vector  $\mathbf{v} \in \mathbb{R}^D$ . This vector

serves as a holistic representation of the image crop, encapsulating its high-level visual concepts. Mathematically,

$$\mathbf{v} = \frac{E_{\text{clip}}^{\text{img}}(\mathbf{I}_{\text{crop}})}{\|E_{\text{clip}}^{\text{img}}(\mathbf{I}_{\text{crop}})\|_2} \quad (14)$$

We provide a detailed description of the node construction process below.

1. **Global Node ( $\mathbf{n}_G$ ):** This node is the simplest, acting as the “anchor” or “context” for the graph. Its feature vector is the L2-normalized global image embedding from CLIP,  $\mathbf{n}_G = \mathbf{v}$ . It grounds the graph in the complete visual evidence of the image crop and represents the holistic concept. The other nodes serve as specialized “attribute descriptors” that refine this holistic view.
2. **Shape Node ( $\mathbf{n}_S$ ):** This node represents the shape concept of the object in the image. It is synthesized through a “predict-and-blend” mechanism. The global feature  $\mathbf{v}$  is passed through a small, learnable MLP head,  $\text{MLP}_S$ . This head acts as a lightweight classifier, outputting logits (raw scores) for  $K_S$  pre-defined shape categories. These logits are passed through a Softmax function to produce a probability distribution  $\mathbf{p}_S \in \mathbb{R}^{K_S}$ , where  $\sum_{i=1}^{K_S} p_{S,i} = 1$ :  $\mathbf{p}_S = \text{Softmax}(\text{MLP}_S(\mathbf{v}))$ . This soft prediction is critical. Instead of making a hard, non-differentiable argmax decision (e.g., “this is 100% a circle”),  $\mathbf{p}_S$  can represent uncertainty or hybrid shapes (e.g., [0.85 (circle), 0.1 (octagon), 0.05 (other)]). We initialize a learnable embedding matrix (a lookup table)  $\mathbf{E}_S \in \mathbb{R}^{K_S \times D}$ . Each row  $\mathbf{E}_{S,i}$  is a  $D$ -dimensional vector that will be trained to represent the “ideal” or “prototypical” embedding for the  $i$ -th shape concept within the CLIP semantic space. The final shape node  $\mathbf{n}_S$  is computed as the weighted average of these ideal shape embeddings, using the predicted probabilities  $\mathbf{p}_S$  as the weights:  $\mathbf{n}_S = \mathbf{p}_S \mathbf{E}_S$ .  $\mathbf{n}_S$  is not just a classification label; it is a synthesized embedding in the  $D$ -dimensional feature space that represents the specific shape-ness of the input image. This process effectively isolates the shape information from  $\mathbf{v}$  and translates it into a vector that is semantically comparable to  $\mathbf{n}_G$ .
3. **Color Node ( $\mathbf{n}_C$ ):** This node is constructed in an identical manner to the Shape Node, but with its own dedicated parameters:  $\mathbf{p}_C = \text{Softmax}(\text{MLP}_C(\mathbf{v}))$  and  $\mathbf{n}_C = \mathbf{p}_C \mathbf{E}_C$ . Here,  $\text{MLP}_C$  predicts a distribution  $\mathbf{p}_C$  over  $K_C$  pre-defined color categories, and  $\mathbf{E}_C \in \mathbb{R}^{K_C \times D}$  is a separate learnable embedding table for these color concepts.  $\mathbf{n}_C$  isolates the color-ness of the object, creating a synthesized embedding (e.g.,  $0.9 \cdot \mathbf{E}_{C,\text{red}} + 0.1 \cdot \mathbf{E}_{C,\text{white}}$ ) that represents the object’s color properties in the shared feature space.

---

**Algorithm 2** LENS-Net Detector
 

---

**Require:** Input images  $\mathbf{I}$  (data), ground-truth boxes  $\mathbf{B}_{gt}$

**Require:** Detector  $\mathcal{D} = \{\Phi_{\text{head}}, \text{backbone}\}$

**Ensure:** Trained LENS-Net Detector  $\mathcal{D}$  and detected bounding boxes  $\mathbf{I}_{\text{crop}}$

```

1: procedure TRAINDETECTOR( $\mathcal{D}$ , epochs, data, freeze_backbone)
2:   if freeze_backbone then
3:     Freeze backbone weights
4:   else
5:     Unfreeze backbone weights
6:   end if
7:   for epoch = 1 to epochs do
8:     for each batch in  $\mathbf{I}_{batches}, \mathbf{B}_{gt}$  in data do
9:        $\mathbf{I}_{\text{aug}} \leftarrow \text{StochasticAugment}(\mathbf{I})$  ▷ Augmentations
10:       $\mathbf{I}_{\text{norm}} \leftarrow \text{Normalize}(\mathbf{I}_{\text{aug}})$  ▷ Normalizes the image to [0, 1]
11:       $z_{\text{raw}} \leftarrow \Phi_{\text{head}}(F_{\text{down}}(\mathbf{I}_{\text{norm}}))$  ▷ Predicts raw parameter vector  $\{\gamma, \alpha, \zeta\}$ 
12:       $p = \frac{\tanh(z_i)+1}{2}(p_{\text{max}} - p_{\text{min}}) + p_{\text{min}}, p \in \{\gamma, \alpha, \zeta\}$  ▷ Transform  $\{\gamma, \alpha, \zeta\}$  in their operational range
13:       $\mathbf{I}_{\text{final}} \leftarrow \text{ApplyDifferentiableTransforms}(\mathbf{I}_{\text{norm}}, p)$ 
14:       $\mathcal{L}_{\text{detect}} \leftarrow \text{YOLOv8Loss}(\mathbf{I}_{\text{final}}, \mathbf{B}_{gt})$ 
15:       $\mathcal{L}_{\text{preproc}} \leftarrow \mathbb{E} \left[ \sum_{i \in \{\gamma, \alpha, \zeta\}} \lambda_i (p_i - p_{\text{default}, i})^2 \right]$  ▷ Equation 3
16:       $\mathcal{L}_{\text{total}} \leftarrow \mathcal{L}_{\text{detect}} + \mathcal{L}_{\text{preproc}}$  ▷ LENS-Net detector's loss function
17:      Backpropagate( $\mathcal{L}_{\text{total}}$ )
18:    end for
19:  end for
20:   $\mathbf{I}_{\text{crop}} \leftarrow \mathcal{D}.\text{Detect}(\mathbf{I}_{\text{final}})$  ▷ Run detection and return crops
21: end procedure
22: Schedule 0: Train head only TRAINDETECTOR( $\mathcal{D}$ ,  $\mathbf{E}_{\text{head}}, \mathbf{I}_{batches}$ , freeze_backbone = True)
23: Schedule 1: Train jointly TRAINDETECTOR( $\mathcal{D}$ ,  $\mathbf{E}_{\text{joint}}, \mathbf{I}_{batches}$ , freeze_backbone = False)
24: return  $\mathcal{D}, \mathbf{I}_{\text{crop}}$ 

```

---

The inherent high class imbalance poses a threat for model to be biased towards the dominant classes. To overcome this, apart from the class-balancing variant of focal loss (Equations 11 and 12), we use a rarity-based augmentation.

**Rarity Based Augmentation.** The probability of applying an augmentation (e.g., photometric, noise, blur) to a training sample from class  $c$  is dynamically scaled based on its rarity  $r(c)$ , where rarity is computed by Equation 15. This ensures that under-represented classes are more heavily augmented.

$$r(c) = 1 - \frac{\log(1 + \text{count}(c))}{\log(1 + \text{count}_{\text{max}})} \quad (15)$$

Each class is assigned an augmentation probability computed using a global base probability of 0.15 and a rarity scaling factor of 0.75 (see Equation 16), ensuring that infrequent classes receive proportionally higher augmentation strength. The same augmentation families used in the detector—photometric jitter, JPEG compression, Gaussian noise, blur, and small rotations—are applied here, enabling consistent robustness improvements across both detection and classification tasks.

$$\mathbf{p}_{\text{class}} = \text{clamp}(\mathbf{p}_{\text{base}} + \mathbf{p}_{\text{scale}} \cdot r(c), 0.05, 0.95) \quad (16)$$

For example, for *parking* class with 22 instances, the rarity score  $r(c)$  is 0.62 and thus  $\mathbf{p}_{\text{class}} = 0.61$ . Similarly, for the *advertisement* class  $r(c) = 0$  and  $\mathbf{p}_{\text{class}} = 0.15$ .

## 10. Additional Results

Table 8 reports the per-class precision, recall, and support across all 41 traffic-sign categories for the LENS-Net classifier, averaged over the five cross-validation folds. We also provide the class-wise performance for Rishabh et al. [50] (the strongest baseline) for comparison. The results show that the LENS-Net classifier maintains strong performance even for classes with extremely limited samples. For rare classes, such as *airport*, *blow\_horn*, *cross\_road*, and *steep\_ascent*, which contain very few (relative to dominant classes) samples per fold, the model achieves non-trivial precision or recall for them. This reinforces the effectiveness of the rarity-aware augmentation strategy and the multimodal fusion components of LENS-Net, which help stabilize learning under class imbalance and data scarcity. In contrast, Rishabh et al. [50] demonstrate substantially poorer performance on these rare categories.

Table 8. Average per-class precision, recall, and support (number of instances) for LENS-Net classifier. The values have been aggregated across five folds.

Class	Precision (%)	Recall (%)	Support
accident	85.47	86.34	102
advertisement	96.18	97.53	3836
airport	100.00	66.74	3
blow_horn	50.00	50.00	2
bus_stop	81.74	83.81	117
cattle	93.31	63.67	22
compulsory_left	92.91	83.96	62
compulsory_right	96.79	93.53	31
cross_road	100.00	100.00	2
direction	88.43	92.66	2777
fuel	86.29	91.55	51
gap	82.87	85.28	164
give_way	90.73	87.28	59
go_slow	91.34	88.27	77
hospital	82.03	47.75	46
left_curve	89.55	82.94	527
men_at_work	95.37	82.07	50
narrow_road_ahead	0.00	0.00	2
no_entry	85.88	72.24	56
no_overtaking	93.13	96.47	199
no_parking	92.44	86.82	188
no_stop_no_stand	95.28	95.27	148
parking	95.00	88.00	21
pedestrian_crossing	87.63	88.29	322
right_curve	82.21	82.95	451
round_about	86.88	82.14	68
school	82.00	76.27	74
side_road_left	87.63	93.28	200
side_road_right	16.79	50.00	3
signal	74.82	53.57	32
speed	93.19	96.00	814
speed_breaker	83.12	80.44	108
steep_ascent	66.71	50.00	8
steep_descent	70.24	62.62	33
stop	93.44	96.73	71
t_intersection	90.00	90.00	19
tampered	84.67	67.28	258
u_turn	87.55	83.34	73
unknown	69.16	61.91	1400
warning	87.04	70.00	34
wide_road_ahead	98.42	84.00	25

A clear trend emerges when comparing different functional groups of traffic signs. Regulatory categories (e.g., *no\_parking*, *speed*, *no\_overtaking*) consistently achieve high scores, supported by the strong geometric and color regularity of these classes. Conversely, signs that frequently appear in visually degraded conditions (such as *hospital*, *gap*, *steep\_descent*, or *side\_road\_right*) exhibit lower recall. These patterns align with the dataset analysis provided ear-

Table 9. Average per-class precision, recall, and support (number of instances) for Rishabh et al. [50]. The values have been aggregated across five folds.

Class	Precision (%)	Recall (%)	Support
accident	81.82	88.24	102
advertisement	93.37	93.20	3836
airport	0.00	0.00	3
blow_horn	0.00	0.00	2
bus_stop	88.03	88.03	117
cattle	86.67	59.09	22
compulsory_left	71.83	82.26	62
compulsory_right	93.55	93.55	31
cross_road	100.00	100.00	2
direction	86.67	90.39	2777
fuel	78.00	81.25	51
gap	67.74	77.30	164
give_way	91.67	89.80	59
go_slow	88.24	58.44	77
hospital	52.38	48.89	46
left_curve	96.86	93.74	527
men_at_work	66.04	70.00	50
narrow_road_ahead	0.00	0.00	2
no_entry	75.00	63.16	56
no_overtaking	93.65	89.85	199
no_parking	82.29	78.26	188
no_stop_no_stand	94.49	83.92	148
parking	46.15	54.55	21
pedestrian_crossing	87.46	79.63	322
right_curve	89.35	91.13	451
round_about	64.29	39.71	68
school	54.17	52.70	74
side_road_left	87.05	84.85	200
side_road_right	100.00	50.00	3
signal	28.85	46.88	32
speed	91.05	94.73	814
speed_breaker	72.55	68.52	108
steep_ascent	100.00	12.50	8
steep_descent	64.29	81.82	33
stop	82.28	89.04	71
t_intersection	66.67	82.35	19
tampered	78.05	63.24	258
u_turn	85.25	71.23	73
unknown	58.26	59.71	1400
warning	86.67	39.39	34
wide_road_ahead	95.45	84.00	25

lier: blur, occlusion, low illumination, and rain degrade the discriminability of certain classes, emphasizing the need for enhancement and robustness strategies when operating in nighttime environments.

Importantly, LENS-Net demonstrates strong robustness to distractor categories intentionally included in INTSD. Classes like *advertisement*, *tampered*, and *unknown* achieve competitive precision and recall, indicating that the GCNN-

based shape/color reasoning and prompt-guided fusion are effective at separating relevant sign content from background clutter, noise, and non-sign elements. This behavior also confirms that the model does not overfit to textural shortcuts, but instead leverages semantically structured cues.

Another insight emerges from the semantic grouping of signs. Shape-based clusters—particularly circular mandatory signs and triangular warning signs—show consistent internal performance, validating our design choice to incorporate explicit shape and color embeddings through GCNN nodes. This suggests that the model’s structural inductive bias aligns well with the underlying visual taxonomy of Indian traffic signs.

## 11. Frequently Asked Questions

### Q: Why do you use 5-fold cross-validation?

The use of stratified 5-fold cross-validation is crucial for several reasons. First, it ensures that each image in the dataset is used for both training and testing, thereby reducing bias in the evaluation process. Second, by averaging the performance metrics across all folds, we obtain a more robust and generalizable assessment of the model’s performance, rather than relying on a single arbitrary train-test split that may not accurately reflect real-world behavior.

### Q: Why did you select a pre-trained and frozen CLIP model?

The choice of CLIP over a standard ImageNet-trained backbone is deliberate as it yields a rich, joint embedding space (a  $D$ -dimensional manifold) where visual and textual concepts with similar semantic meaning are projected to nearby locations. Freezing the model preserves its generalized knowledge [36], prevents overfitting, and enables efficient training of the LENS-Net classifier.

### Q: How are CLIP embeddings useful in traffic sign classification?

CLIP embeddings are useful because they are trained on large, diverse datasets and therefore bring robustness to variations such as lighting, scale, and moderate occlusion, all common in traffic scenes.

### Q: How is $f_{CA1}$ relevant?

$f_{CA1}$  represents the first-stage fusion between the CLIP image embedding and the text-prompt embeddings. It captures how the image features align with semantic priors expressed in the prompts—such as shape, color, icon type, and sign function. This alignment enriches the global image embedding with high-level contextual cues that CLIP alone may not emphasize, especially under noise, blur, or low-light conditions. As a result,  $f_{CA1}$  provides a semantically informed representation that guides the

subsequent node construction and GCNN processing, ensuring that the later fusion stage ( $f_{CA2}$ ) operates on features that already encode text-conditioned structure relevant to traffic sign recognition. Conceptually, it aligns the image’s representation with the kinds of textual distinctions that are useful for traffic-sign recognition (e.g., color/shape descriptions, presence of numbers or arrows, etc.).

### Q: Why do you normalize the adjacency matrix symmetrically?

We symmetrically normalize the adjacency matrix in the GCNN to ensure stable and well-behaved message passing across the graph. In its raw form, the adjacency matrix can lead to disproportionate aggregation, where nodes with high degree dominate the feature propagation. It also improves training stability and convergence.

### Q: How is $f_{CA2}$ relevant?

$f_{CA2}$  is highly relevant because it captures: (i) **Global semantic information** from the original CLIP embedding, (ii) **Fine-grained geometric and chromatic cues** aggregated through the shape and color nodes, (iii) **Contextual reasoning** obtained by querying GCNN-refined node features through cross-attention, and **Prompt-based textual priors** incorporated earlier in CA1.

By combining these complementary modalities,  $f_{CA2}$  forms a richly structured, semantically aligned embedding that is significantly more discriminative than any single source alone. Hence, it serves as the input to the final classifier, making it the key representation upon which the model’s prediction relies.

### Q: What is the effect of using answers to the predefined prompts as textual embeddings $T$ instead of the static prompt embeddings $P$ ?

We also experimented with replacing the fixed prompt embeddings  $P$  with dynamically generated textual descriptions obtained from a BLIP image captioner. These caption-based embeddings  $T$  did not yield any meaningful improvement in accuracy, while substantially increasing computation. Consequently, we retain the more efficient static prompt-based embeddings in our final design.

### Q: What happens if we use a simple CNN as classifier?

We also trained a simple CNN using the same hyperparameters, but the performance was suboptimal. It achieved an A.P. of 27.10%, A.R. of 22.17%, and accuracy of 60.56%.